Particles II

Access the latest eBook →

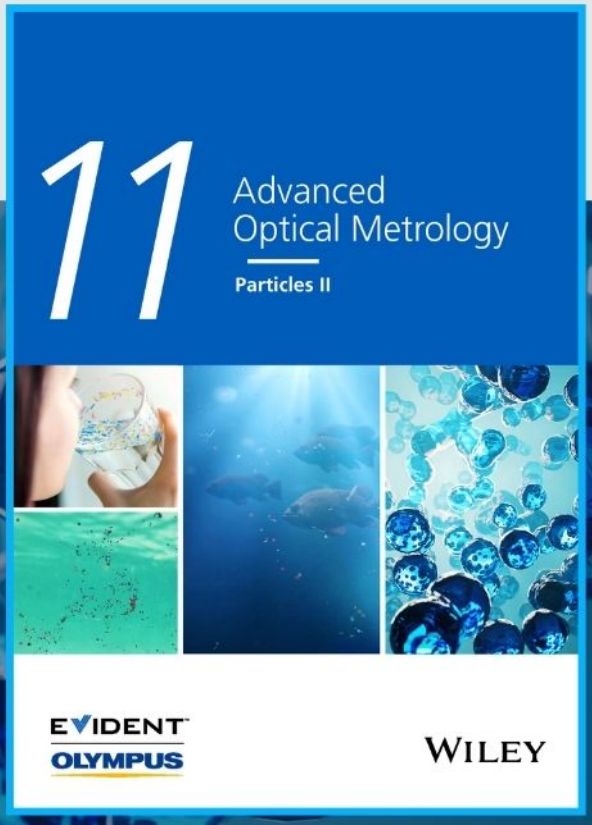

Impact on Biological Systems and the Environment

This eBook is dedicated to the research of Professor David Wertheim.
In collaboration with various groups, Professor Wertheim uses confocal microscopy to analyse the impact of different types of particles on human health and the environment, with a focus on human health-hazardous particles detected with solid-state nuclear track detectors (SSNTD). Download for free, today.

EVIDENT
OLYMPUS

WILEY

ADVANCED MATERIALS INTERFACES
www.advmatinterfaces.de

Red Carbon Thin Film: A Carbon–Oxygen Semiconductor with Tunable Properties by Amine Vapors and Its Carbonization toward Carbon Thin Films

Paolo Giusto, Daniel Cruz, Yael Rodriguez, Regina Rothe, and Nadezda V. Tarakina*

The requirements for organic semiconductor materials and new methods for their synthesis at low temperature have risen over the last decades, especially due to concerns of sustainability. Herein, the synthesis of a carbon/oxygen molecular semiconductor thin film, which is promptly reactive toward amines, is presented. This allows for tuning the semiconductor properties and application as amine vapor sensors for a scope of analogous amines. The gas-to-solid phase reaction causes a significant change of the films' optical properties, blue-shifting the absorption and the photoluminescence spectra from the red to the near UV spectral range. The irreversible chemical reaction between the thin film and the amine vapor is also exploited for the preparation of nitrogen-containing thin carbon films. The herein presented materials and methods will be of interest for gas sensing applications as well as for the development of tunable semiconductors and heteroatom-doped thin films.

1. Introduction

Increasing requirements for high-performing devices raise concerns regarding the supply of raw materials, especially regarding rare metals and semiconductors. For this reason, much effort has been devoted to the development of alternative materials based on carbon. The development of new synthetic techniques and the strong advances in characterization methods enabled a new era in materials science around carbon. Known materials such as carbon nitride experienced a strong comeback, and new materials classes with extraordinary properties were explored, such as ternary boron carbon nitrides, C_2N, and more.[1–6] Recent research focused especially on the introduction of nitrogen into covalent sp^2-hybridized structures, with less attention paid to materials composed of carbon and oxygen.[7]

Beyond the most common carbon monoxide (CO) and carbon dioxide (CO_2), there is a series of less known carbon oxide linear compounds with general formula C_nO_2 ($n \geq 1$). Among those, carbon suboxide (C_3O_2) is an industrial product used at the ton scale in the early 20th century which attracted attention as a highly reactive synthon for the synthesis of heterocycles and malonyl derivatives.[8,9] C_3O_2 behaves like a bisketene and was described by Kappe and Ziegler as a "double dehydrated malonic acid".[9]

In the last century, various methods for the synthesis of carbon suboxide have been investigated (**Figure 1**).[9,10]

Carbon suboxide is a metastable gaseous molecule with low melting (–112.5 °C) and boiling (6.8 °C) points.[11] Its structure was recently resolved showing slight deviation from linearity and alternated charges which are the primary reason for its high reactivity, having a strongly negative charged carbon at C^2 surrounded by two positively charged carbon atoms (C^1 and C^3).[11,12] Besides the interest in organic synthesis, carbon suboxide attracted attention also in materials science, since the molecule readily reacts forming the so-called poly(carbon suboxide) or "Red Carbon", for its dark, wine red appearance.[12] For the red carbon materials many different structures have been proposed, however, without being finally resolved.[11–14] Furthermore, the red carbon has been always reported in the form of bulk material, that is, obtained by bulk polymerization. However, the properties of red carbon make it highly attractive for the development of functional thin films.

Thin film technology is widely used to improve the performances of bulk materials, such as anti-corrosion and anti-wear, or self-cleaning properties, while using a very low amount of raw materials. The production of sensors is of particular interest especially for food safety, which became recently one of the most important global issues. Every year, the inappropriate handling and the consumption of spoiled food causes serious problems to millions of people all over the globe.[15] In many cases, the presence of biogenic amines, such as putrescine or cadaverine produced by the breakdown of amino acids, indicates the microbial spoilage of food.[16] These biogenic amines are highly volatile compounds, which are therefore detectable by chemical and/or physical sensors which could help identifying issues in

P. Giusto, Y. Rodriguez, R. Rothe, N. V. Tarakina
Max Planck Institute of Colloids and Interfaces
Department of Colloid Chemistry
Am Mühlenberg 1, 14476 Potsdam-Golm, Germany
E-mail: paolo.giusto@mpikg.mpg.de
D. Cruz
Fritz–Haber-Institute of the Max Planck Society
Dept. Inorganic Chemistry
Faradayweg 4–6, 14195 Berlin, Germany
The ORCID identification number(s) for the author(s) of this article can be found under https://doi.org/10.1002/admi.202200834.

DOI: 10.1002/admi.202200834

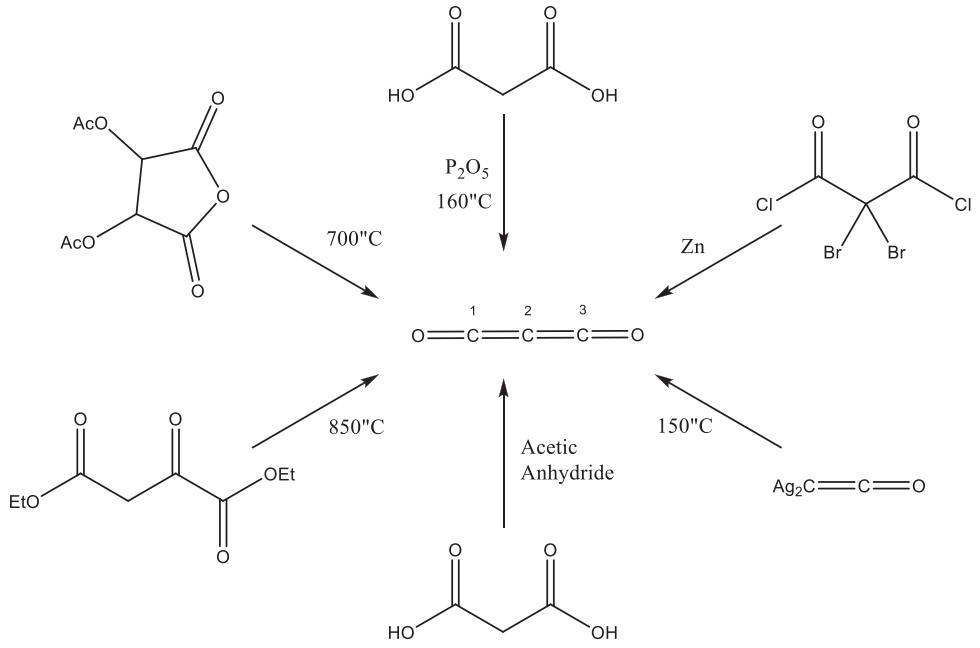

Figure 1. Summary of synthetic methods for carbon suboxide.

the delivery chain early on.[17] Among the methods used for the detection of biogenic amines, optical methods provide a reliable and fast response with simple setups.[18] Recently E-noses for food spoilage, using mostly cross-reactive metal oxides and colorimetric sensor arrays have been successfully employed.[19] However, the use of metal oxide-based E-noses generally require high temperatures, are humidity sensitive, and cannot distinguish closely similar compounds.[20] Therefore, non-metal-based sensing materials would be of high interest. Yet, due to the limited options of suitable precursors, the synthesis of such films has been challenging until today.

Herein, we developed the synthesis of functional thin films from gas-phase reaction of carbon suboxide and, based on experimental evidences, we attempt to define the red carbon structure. The synthesis of red carbon thin films exploits a solid mixture of malonic acid (MA) and phosphorus pentoxide (P_2O_5) in a test tube placed in a muffle furnace at 160 °C. The choice of using MA and P_2O_5 mixture enables to synthesize the gaseous carbon suboxide which further reacts to red carbon films at the substrate surface. The obtained red carbon thin film, hereafter defined as "molecular Red Carbon" (m-RC), to highlight the difference with respect to the polymer structures, is demonstrated to be a semiconductor material that can act as an optical sensor to distinguish similar amines, even by naked eyes. The exposure to amine vapors causes an irreversible change in the optical properties, such as absorption and fluorescence. The change in optical properties enables to use these materials not only as sensitive and selective sensors, but also as a platform for tuning optical properties over the whole visible spectrum.

2. Results and Discussion

The m-RC thin films are synthesized from a solid mixture of solid precursors, MA and P_2O_5. The mixture is transferred in a test tube with a glass slide serving as a target substrate and then placed horizontally in a muffle furnace at 160 °C. At this temperature, P_2O_5 double-dehydrates the MA producing the carbon suboxide gas, obtained by removing the hydroxyl groups and the α-hydrogens, which are typically acidic in β-diketo compounds. After the thermal treatment, the glass substrate is successfully coated on both sides with a thin film of deep-red color, which resembles the description in previous reports on bulk red carbon materials (**Figure 2**a,b).[12,21,22] In the present case, the red color is confirmed by the absorption spectrum (Figure 2c, black line), where the m-RC thin film presents an absorption maximum at 363 nm with a long shoulder over a wide range of the visible spectrum and an optical bandgap of 2.1 eV (Figure S1, Supporting Information). Furthermore, the RC films display an intense red fluorescence at 675 nm (Figure 2c, red line). The as-prepared films are smooth and homogeneous on the glass surface, as confirmed by scanning electron microscopy (SEM) and atomic force microscopy (AFM), with an average thickness of 28 nm (Figure S2, Supporting Information). Furthermore, the material presents relatively high thermal stability, up to 200 °C in N_2, and a residue of about 21% at 1000 °C (Figure S3, Supporting Information), suggesting the possibility to exploit m-RC thin films as a platform to prepare carbon-rich thin films as it will be shown in a later part of this work. In order to confirm that the film is homogeneously composed of carbon and oxygen, we performed energy-dispersive X-ray spectroscopy (EDX) (Figure 2d) mapping of the film surface where parts of the film were removed during the sample preparation. The analysis of the EDX results reveals that the film is mostly composed of carbon and allegedly a lower contribution of oxygen. Furthermore, the silicon EDX mapping shows that the film is homogeneous, since a high intensity signal for the silicon occurs only where the film has been removed during the sample preparation. The analysis also confirms the absence of phosphorus contamination whose peak (P-K) usually occurs at

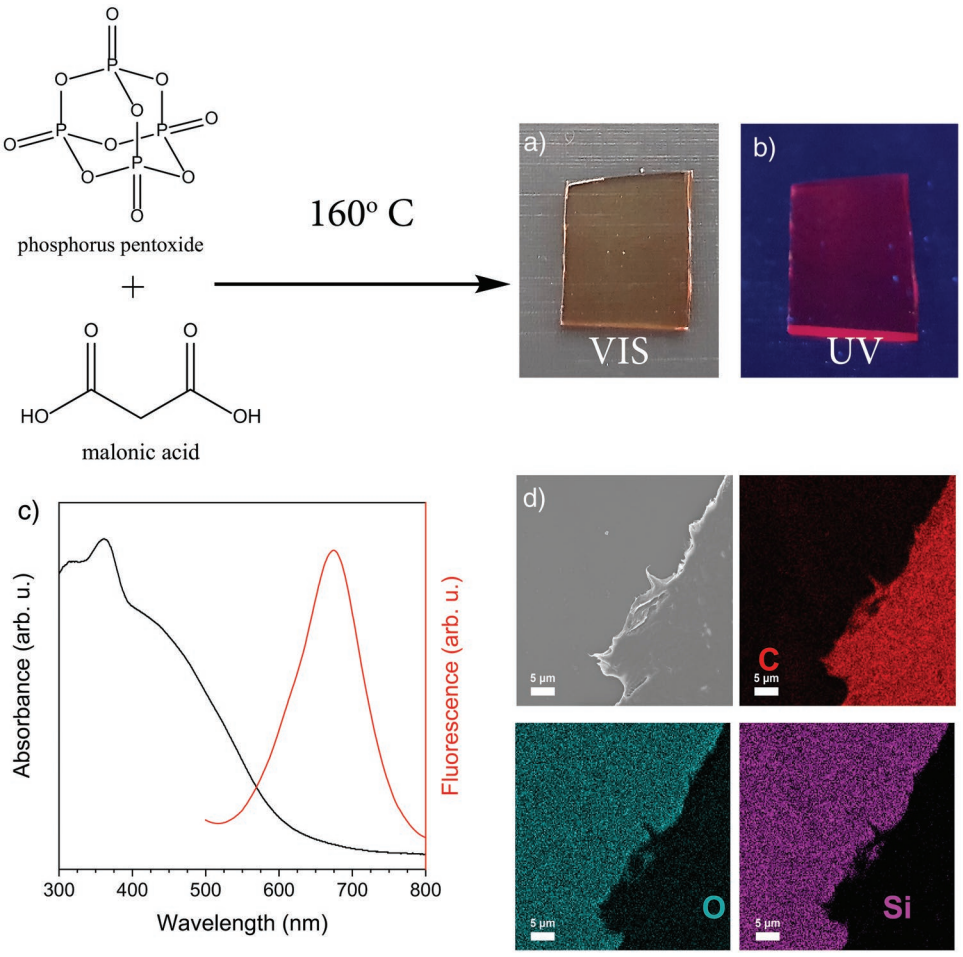

Figure 2. Synthesis of m-RC thin films: a,b) pictures of the m-RC thin films under ambient and UV illumination; c) absorbance and fluorescence spectra; d) secondary electron SEM image and corresponding EDX maps of C, O, and Si signals (intensity scale in Figure S4, Supporting Information).

2 keV (Figure S4, Supporting Information), meaning that the P_2O_5 is not evaporating and it is kept as leftover at the bottom of the test tube after the reaction is completed.[23] To obtain preliminary information on the material structure, the m-RC films were analyzed by Fourier-transform infrared spectroscopy (FTIR) (Figure S5, Supporting Information). The spectrum confirms the presence of carbonyl-containing groups, occurring at 1728 cm^{-1} is attributed to ester-like functional groups, with negligible contributions of C–H- and O–H-containing groups (3500–2700 cm^{-1}).

To get more insights on the crystal structure and chemical composition, we used a combination of X-ray powder diffraction (XRD), transmission electron microscopy (TEM), X-ray photoelectron spectroscopy (XPS), and electron energy loss spectroscopy (EELS) (**Figure 3**). The first two methods provide structural information on the material, which, in combination with XPS and EELS, enables to elaborate the chemical structure of the m-RC material. The XPS of m-RC C1s (Figure 3a) shows the presence of five different bonding scheme present in the material, with a significant majority of C = C bonds with sp^2 hybridization (at 285.2 eV), which account for the 58.4% of the total C bonds. Among the C–C bonds, also the ones with sp^3 hybridization (286.1 eV) are present, with about 21.3% relative occurrence, with a total overall of about 80% of C–C bonds. The rest 20% is composed by C–O bonds, with ether configuration (10.7%, at 287.4 eV), carbonyls (5.8%, at 288.5), and ester (3.8%, at 289.7 eV), as confirmed by the O1s spectrum (Figure 3b). Also from XPS analysis we couldn't detect any contamination from phosphorus. The relative composition of the m-RC samples in terms of C/O ratio is 5:1 from XPS, in good agreement with EDX data (Figure S6, Supporting Information).

The XRD patterns of the as-deposited films on the glass show no specific features, resembling the pattern of the bare glass substrate (Figure 3c, blue and grey line, respectively). In parallel the m-RC thin films were also dispersed in tetrahydrofuran (THF) and dropped directly at the surface of the silicon XRD holder (hereafter referred as m-RC–THF). The m-RC–THF sample shows then sharp peaks on the XRD diffraction pattern (Figure 3c, black line), which can be indexed in a trigonal unit cell with unit cell parameters $a = b = 16.4$ Å, $c = 9.36$ Å. The sharp and well-defined diffraction peaks confirm the molecular size of the red carbon prepared here. In order to address the structure and chemistry at the nanoscale, a detailed TEM analysis of the m-RC–THF samples was performed. The m-RC–THF samples consist of at least two different phases: 1) large C- and O-containing flakes and 2) hollow carbon onion

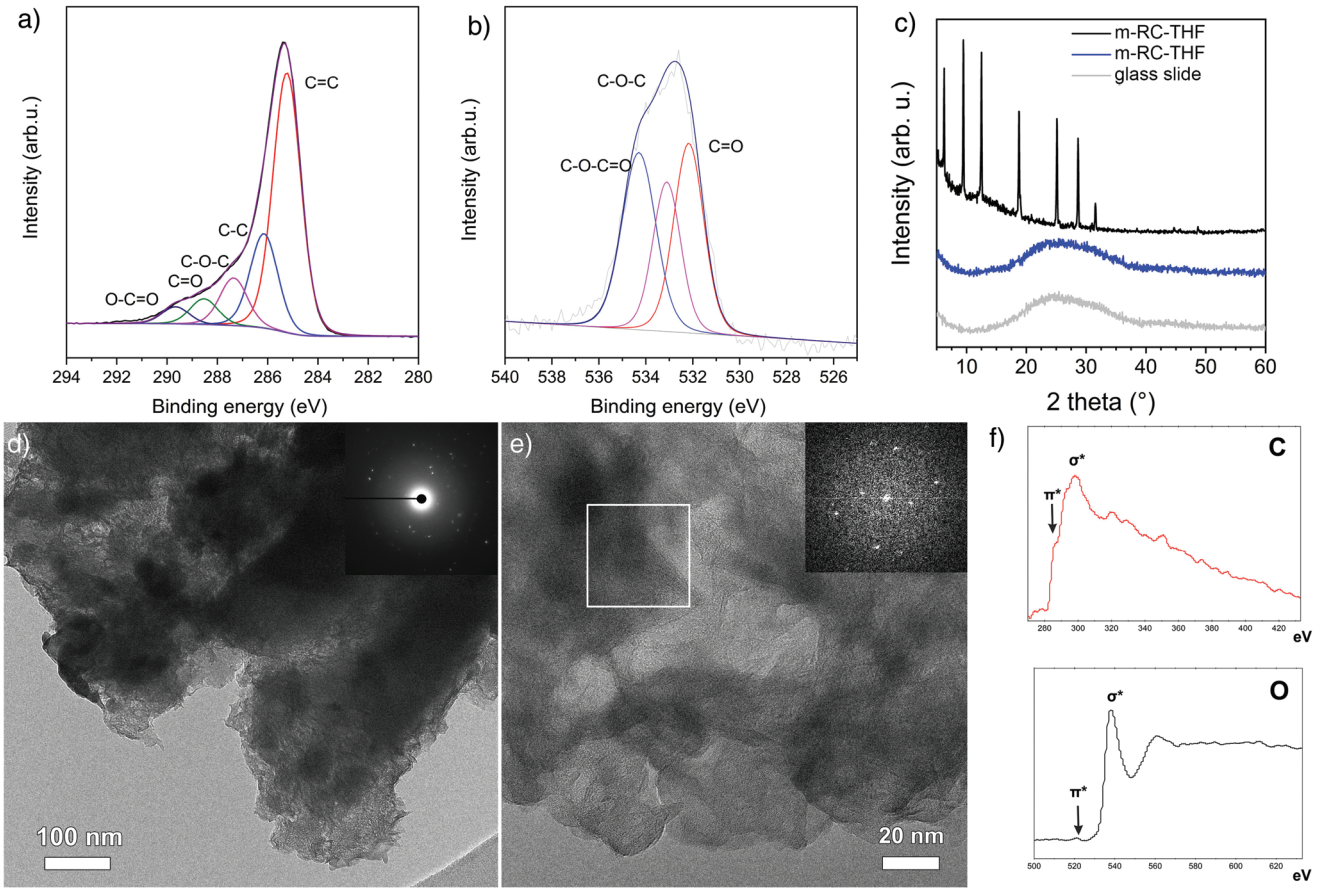

Figure 3. Structural and chemical characterization of m-RC thin films. Deconvoluted XPS spectra of m-RC thin films: a) C1s and b) O1s; c) XRD of bare glass slide (grey line), m-RC on glass (in blue), and m-RC–THF casted on the XRD holder (in black); d,e) HR-TEM pictures of m-RC–THF (FFT in insert) and f) EELS high loss spectra of C and O K-edges.

agglomerates (Figure 3d,e and Figure S7, Supporting Information, respectively). The latter displays typical features of graphitic-like carbon materials at the C K-edge EELS spectra in absence of oxygen.[24] Fast Fourier transforms (FFT) obtained from high-resolution TEM images of the hollow carbon onion agglomerates show a broad (002) and a sharp (111) peak resembling graphitic carbon structures.[25,26] In case of large flakes both C and O signals are present on EELS spectra (Figure 3f): The C K-edge has a very low intensity π^*-peak and a σ^*-peak displaying fine structural features; the O K-edge has only a σ^*-peak without specific fine structure features. High resolution TEM (HRTEM) images and FFT patterns confirm that these flakes consist of an amorphous matrix (diffuse signal on SAED patterns) with crystalline inclusions (sharp peaks on SAED patterns). The interplanar distances obtained from the XRD peaks are in good agreement with the 2θ peaks at 12.8° (0.68 nm), 25.1° (0.34 nm), and 28.6° (0.32 nm) on the XRD pattern. Since the peaks on the XRD pattern appear after dispersing the film we postulated that THF may induce the crystallization of the material.

The starting model to describe the XRD pattern was built starting from previous attempts to describe red carbon materials as nanobelts, finding a good match with our experimental results.[27,28] Therefore, by combining our observations and previous reports we constructed several types of derivatives: cyclohexameric, cyclooctameric as well as C_3O_2/C_5O_2 hexacycles (**Figure 4**). Several structural models based on these molecular belts were built. The best fit to the XRD pattern was observed for the model with $(C_3O_2/C_5O_2)_3$ hexacycles (Figure S8, Supporting Information). In this structural model, which combines all the insights obtained from previous characterization, depicts the material as composed by carbon rich rings ended with α-pyrone units at the edges. This model and a modification of it with THF molecules introduced into the empty channels in between rings were used as a starting point to perform a classical simulated annealing with the EXPO2014 software package.[29] The complexity of the obtained material does not enable us, at this stage, to convey unambiguously the chemical composition of the crystalline phase in spite of the considerable improvement of the XRD pattern fit (Figure S8, Supporting Information). In order to further improve the current structural model, additional studies of the crystallization and the exact composition of the obtained phase are required, and will be the subject of a future, more detailed investigation.

m-RC was reported to be highly reactive to ammonia and, therefore, we exploited the possibility to use the m-RC thin films as sensing platform for amines, which will enable the

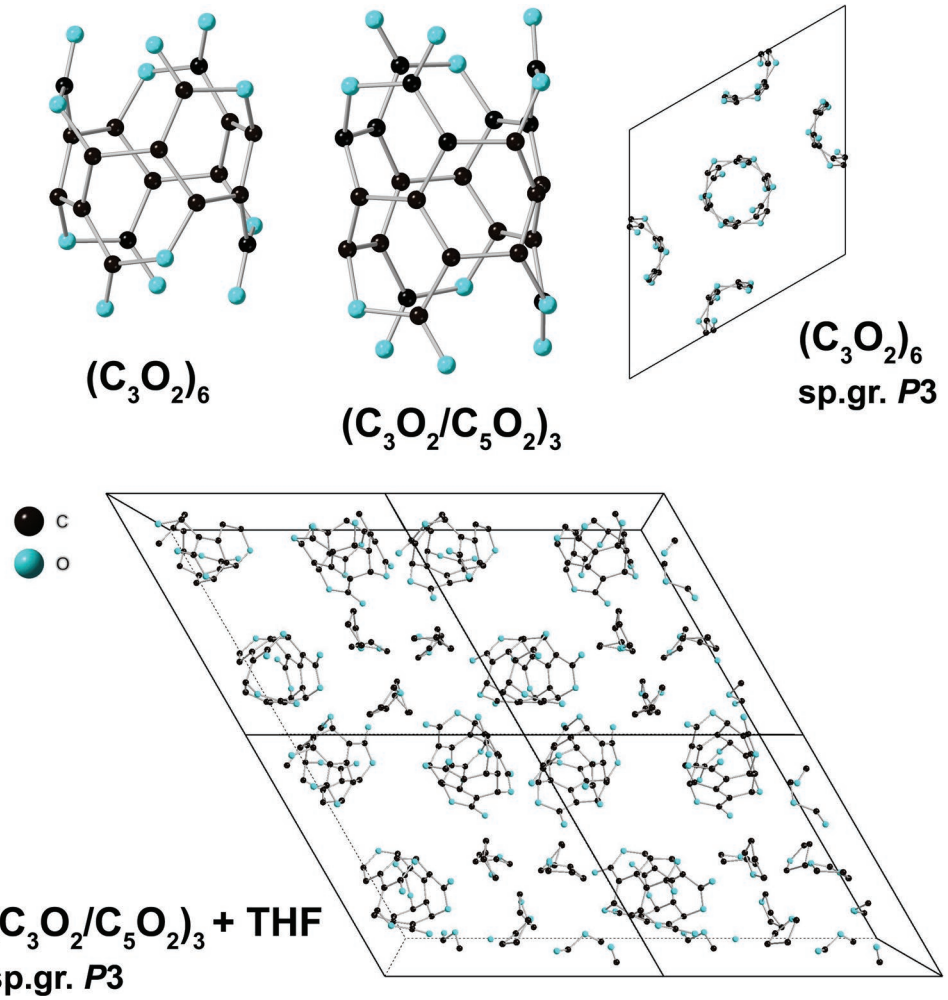

Figure 4. $(C_3O_2)_6$ and $(C_3O_2/C_5O_2)_3$ clusters and two crystal structure models constructed using these clusters.

control of the optical properties via gas-solid interaction.[12,22] For this purpose, we chose a set of analogous alkylamines, mono-, di-, tri-ethyl and benzyl-, and an aromatic amine, that is, aniline. In a home-made setup we put 1 mL of an amine in a 100 mL vessel (total volume 134 mL) and immediately sealed, after placing inside a 1×2.5 cm^2 m-RC thin film in another 5 ml vessel, to avoid direct contact of the sample with the liquid amine (Figure S9, Supporting Information). In this way we assure that the interaction between the gas and the solid film occurs only via gas-to-solid phase. After 24 h of exposure m-RC thin film displays significant color changes, which can even be distinguished by naked eyes (as shown in Figure S9, Supporting Information). The color changes were recorded via UV–vis spectrometry at time intervals between 0.05 (i.e., 30 s) and 48 h at arbitrarily chosen points in time (30 s, 5 min, 30 min, 1 h, 4 h, 13 h, 24 h, and 48 h) for each amine (Figure S10, Supporting Information) and further elaborated to obtain the bandgap values over time (**Figure 5**a, values are listed in Table S1, Supporting Information). As expected, the kinetics of the color change is faster for more volatile amines due to their higher vapor pressure. Indeed, with $EtNH_2$ a strong absorption blue-shift occurs already after 30 s of exposure (from 2.10 of the bare m-RC to 2.52 eV). After just one hour of exposure we recorded a bandgap size increase, which is larger for the primary amines (2.78 eV for $EtNH_2$, 2.61 eV for benzylamine), followed by secondary, tertiary aliphatic amines, and lowest for the aromatic amine, that is, aniline (2.3 eV). The trend is confirmed also for longer exposures of 48 h: Primary amines enable larger blueshift of the absorption edge. Therefore, the final absorption blueshift, and the relative widening of the bandgap, do not depend on the amine vapor pressure, but to the chemical properties of the amine. Indeed, the boiling point of the ethylamine ($EtNH_2$) is 16.6 °C, whereas the one of benzylamine (which is as well a primary amine) is 185 °C (at atmospheric pressure), which causes the first to have the fastest color change kinetics, but a similar change after 48 h. Indeed, $EtNH_2$ enables a very large bandgap blue shift of 1.14 eV (from 2.10 of bare m-RC to 3.24 eV after 48 h) and 0.87 eV for benzylamine (2.97 eV after 48 h), whereas for aniline only 0.47 eV (2.59 eV after 48 h exposure). In this way, we can rule out the predominant effect of the vapor pressure on the thermodynamics of the response, that is, when vapor pressure equilibrium condition is reached, since benzylamine and aniline have comparable boiling points. Concerning the

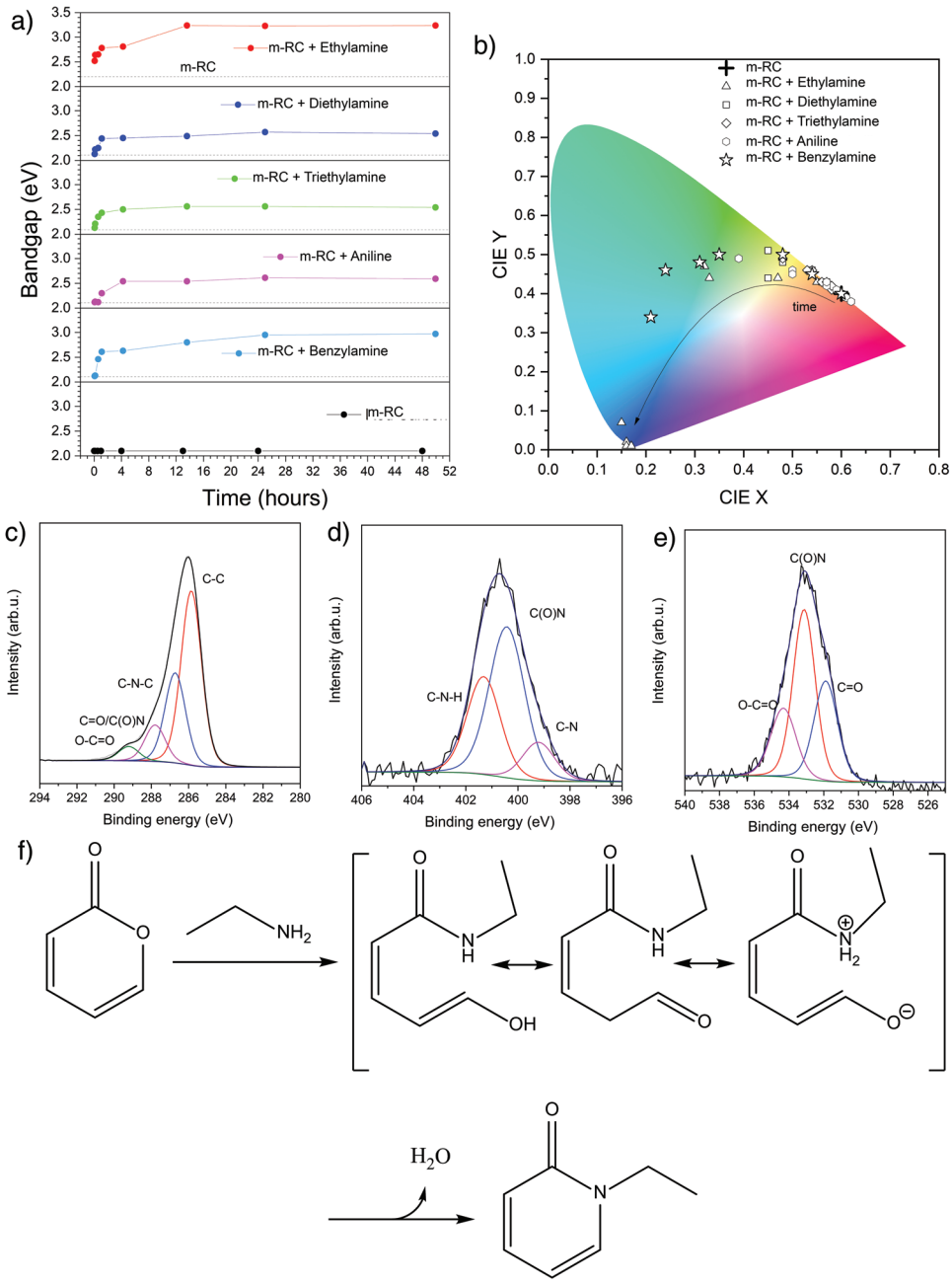

Figure 5. a) Bandgaps and b) fluorescence of m-RC thin films sample at different times of exposure to selected amines; c) C1s, d) N1s, e) O1s XPS deconvoluted spectra of m-RC–$EtNH_2$; f) proposed mechanism for the chemical reaction of m-RC with $EtNH_2$.

other amines, the bandgap widening is similar after 48 h, with a maximum total variation of 0.41 eV. The irreversibility of properties change is confirmed by placing the sample exposed to $EtNH_2$ vapors for 24 h in a vacuum over for 20 h at 60 °C and measuring the absorption spectrum which did not change (Figure S11, Supporting Information), suggesting that a chemical reaction between the amine and the m-RC occurs. Besides the possibility to distinguish compounds with similar chemical–physical properties, the method herein presented reveals the possibility to tune the optical properties of this material over almost the whole visible spectrum. Eventually, we would expect that other volatile compounds would enable a different blue- (or red-) shift of the optical properties, as well as, an irreversible incorporation in the material of the chosen element, such as boron, sulfur, and more.

As previously mentioned, m-RC thin films possess a strong fluorescence in the red spectral range (675 nm). Therefore, another very attractive opportunity is the tuning of the photoluminescence emission. As expected, photoluminescence also blueshifts, more for $EtNH_2$ and benzylamine than for other amines, in good agreement with the absorption spectral blueshifts. In the first case, after 48 h of exposure, ethylamine

causes a shift of the photoluminescence from 675 nm of the bare m-RC down to the near UV range (384 nm) (Figure S12, Supporting Information). In the second one, benzylamine shifts the fluorescence in the cyan region, with a maximum at 499 nm. The blueshift is less strong for diethylamine, trimethylamine, and aniline, analogously to the absorption spectrum, shifting the maxima "only" from 65 to 80 nm to the orange spectral range (≈595–610 nm). It is worth noticing, that in this way the m-RC thin films and its amino-sensed derivatives enable covering almost the full color spectral range, from the red, through yellow, green, and cyan, down to the deep blue and even near-UV spectrum, blue-shifting more for longer exposure times and for primary amines, as exemplarily shown by the CIE 1931 graph (Figure 5b). Such a wide range of bandgap size and photoluminescence tunability gained recently a lot of attention for application in optoelectronics, optical sensors, and bioimaging with other materials.[30,31] Therefore, we assume that the herein presented m-RC thin films can take an important share in the above applications.

Last but not least, the m-RC/amine interaction can be followed also by FTIR. Exemplarily, the strong absorption of the carbonyl group, shifts toward lower wavenumbers, confirming that a reaction occurs between the ester group (1730 cm^{-1}) that is converted into an amide (1650 cm^{-1}) for $EtNH_2$ already after 30 s (Figure S13, Supporting Information). In order to prove whether the sensing mechanism and the tuning of the optical properties occur due to a chemical reaction we further characterized the sample exposed to $EtNH_2$ for 24 h (m-RC–$EtNH_2$-24). The surface morphology, evaluated by SEM, reveals that the exposure to $EtNH_2$ vapors causes the formation of some "wrinkles-like" surface defects attributed to the chemical reaction, and by means of EDX we could show that the N is successfully present into the thin film material (Figure S14, Supporting Information). In terms of thermal stability the m-RC–$EtNH_2$-24 show a large leftover product at 1000 °C (25.5% in nitrogen atmosphere).[32] XPS can provide further insights in the materials structure for m-RC–$EtNH_2$-24 (Figure 5c–e). In good agreement with FTIR, the reaction with $EtNH_2$ leads to the formation of amide bonds (287.8, 400.4, and 533.1 eV) accompanied by a significant reduction of the ester bond signal. Furthermore, a deconvoluted peak attributed to –NH groups, appearing also in the FTIR spectrum (Figure S15, Supporting Information), shows that the reaction proceeds via pyrone ring-opening, at the edge of the nanobelt in Figure 4, which would eventually close via elimination of water to pyridinone (Figure 5f). Therefore, the intermediate ring-opening would explain the blue-shift in absorbance and fluorescence, since the main product (the intermediate) has a reduced conjugation length with respect to the closed form. We can assume that the intermediate is the major reaction product, because of the intense –NH signal in XPS and FTIR. Additionally, XPS enables to derive the relative elemental composition as $C_{15}NO_2$ (C 83.6%, O 11.0%, and N 5.4%) confirming thus the partial substitution of oxygen with nitrogen (C/O = 5.1≈ $C_5O = C_{15}O_3$; $C_{15}O_3 - 1*O+1*N = C_{15}NO_2$), by means of the $EtNH_2$ vapor.

TGA profile of the bare m-RC and m-RC–$EtNH_2$-24 (Figure S16, Supporting Information), reveals the possibility to prepare carbon materials as thin films, while selectively introducing nitrogen functionalities. SEM analysis confirms that the film is still present after treatment at 400 °C, with some surface defects occurring due to the thermal process (**Figure 6**a,b and Figure S17, Supporting Information). Furthermore, C, O, and N signals are present on the EDX spectra of the sample exposed to $EtNH_2$. The absorbance spectra show an increased optical absorption in the visible range for the bare m-RC film further condensed at 400 °C, whereas a high transparency for the one exposed to $EtNH_2$ was preserved. FITR shows a quite low absorption for both samples, in the range 4000–1300 cm^{-1}. In both samples, however, three features can be easily distinguished and attributed to C = C bonds (1600 cm^{-1}), condensed allene bonds that appears as a doublet at about 1970 and 2015 cm^{-1}, and ketene units at 2179 cm^{-1} (Figure S18, Supporting Information).[33] The XPS spectra confirm that at 500 °C, the samples are still present, and up to 400 °C part of the nitrogen remains in the structure. To investigate the thermal mechanism of the formation of the carbon films the samples, m-RC and m-RC–$EtNH_2$-24 were analyzed by *operando* XPS. The spectra of m-RC clearly show that the thermal treatment modifies the chemical environment during heating (Figure 6d). The major sp^2 C–C peak shifts to lower binding energies, from 285.0 to 284.4 eV, which therefore speaks for significantly more electron rich C–C bonding scheme. The more oxidized peaks, reduces in intensity and remain as a tail up to 500 °C. Analogously, the O1s spectra recorded at different temperatures reveal the appearance of the SnO (≈531 eV) attributed to a thinning and eventually cracks of the film occurring during the carbonization (Figure S19, Supporting Information). However, the peak attributed to carbonyl carbon is still present at 532.1 eV even at 500 °C, with a final C/O ratio of about 42 (97.67% C, 2.33% O). The increased condensation and the successful carbonization of the film are confirmed also by the picture of the sample at 500 °C, where the color turns darker and the absorption increases accordingly in the whole visible spectrum (Figure S20, Supporting Information). To evaluate the possibility of creating N-doped carbon thin films by this method we performed analogous experiment for m-RC–$EtNH_2$-24. Analogously to the case of the m-RC film, a major change in the C1s spectrum appears at 300 °C, where the main peak progressively shifts from 285.5 eV (at room temperature) to lower binding energies (284.7 eV at 300 °C) reaching 284.4 eV at 500 °C, with the other peaks fading in a low intensity tail (Figure 6e). The O1s peak reveals similar behavior, with the appearance of the peak attributed to the SnO substrate, due to thinning and cracks formation during the carbonization (Figure S19, Supporting Information). When raising the temperature, the N1s peak is present and clearly detectable until 400 °C, whereas at 500 °C cannot be detected anymore (Figure 6f). The thermal treatment induces also for the nitrogen a major change between 200 and 300 °C, with the appearance of a feature at lower binding energies (398.2 eV) together with the amide bond at 400.4 eV. The 398.2 eV feature attributed to pyridinic nitrogen confirms the introduction of nitrogen within the material structure.[34] It is worth pointing out that in this case the material obtained at 400 °C has a high transparency in the visible range as confirmed by the sample picture and absorbance spectrum (Figure S20, Supporting Information). Furthermore, we could define the CNO composition (excluding the oxygen attributed to the substrate) as ≈$C_{27}NO$ (92.82% C, 3.39% N, and 3.79% O) (Figure 6).

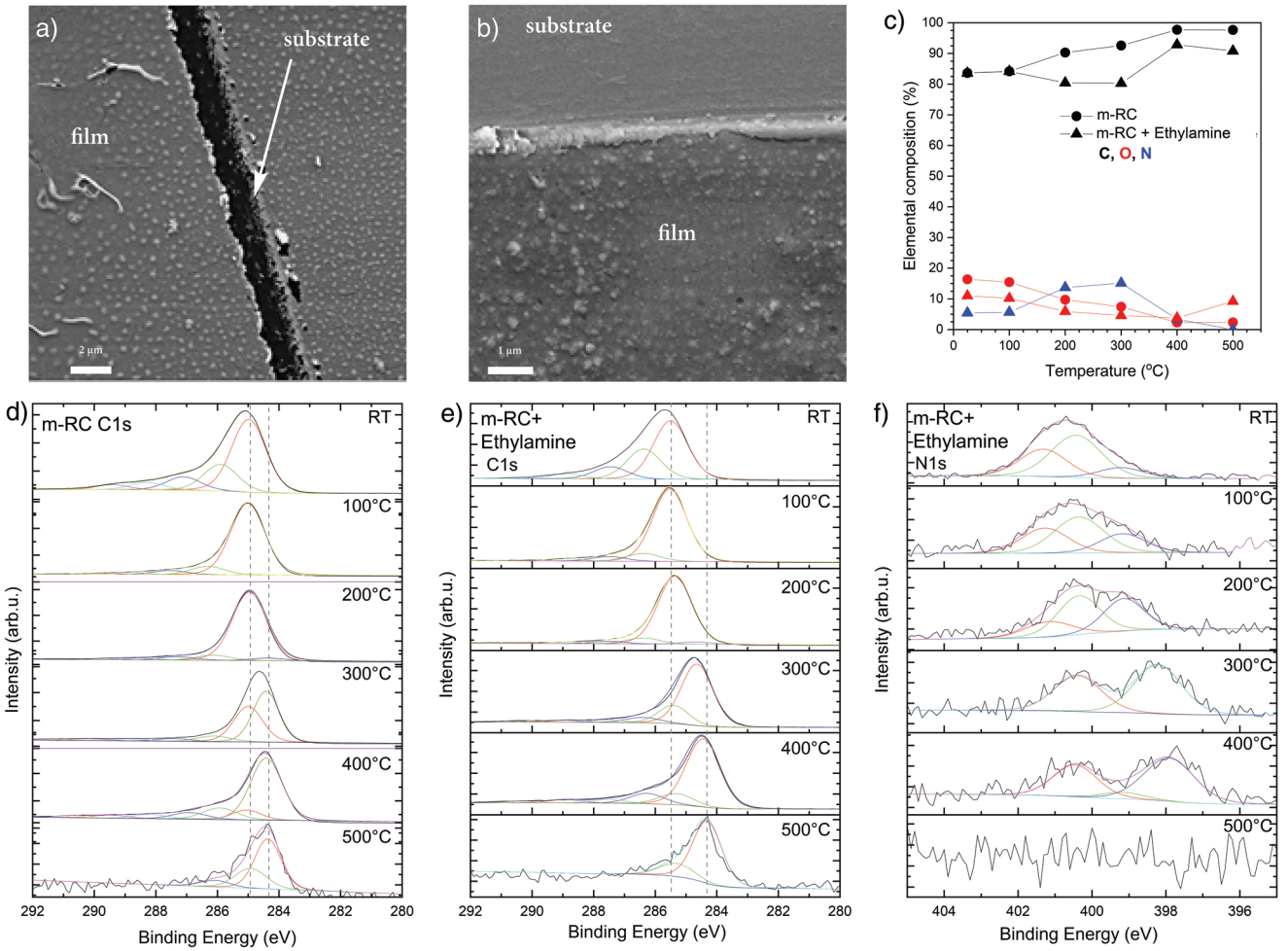

Figure 6. a,b) SEM of m-RC and m-RC + $EtNH_2$ at 400 °C. c) Relative chemical composition at different temperatures, obtained by operando XPS. d) m-RC C1s, e) m-RC-$EtNH_2$ C1s, and f) N1s Operando XPS of m-RC and m-RC + $EtNH_2$.

However, when increasing the temperature to 500 °C, the nitrogen peak cannot be detected anymore, and the leftover film is composed only by carbon and oxygen with a C/O ratio of 9.9 (90.8% C, 9.2% O), different from the bare m-RC film. The relative elemental composition study at different temperatures reveals the possibility to control tightly the elemental composition in the material and, therefore, the material properties. In good agreement with the TGA, until 100° the sample does not change, the composition remains constant (Figure 6c). Minor changes occur at 200–300 °C and we see a different behavior between the two samples: In the m-RC film, the C% increases where the oxygen decreases, whereas in the m-RC + $EtNH_2$, N% increases at the expenses of oxygen and nitrogen. At 400 °C the carbon content increases significantly for both samples reducing the heteroatoms content, with minor changes at 500 °C for m-RC. In the case of m-RC + $EtNH_2$, the step between 400 and 500 °C causes the complete removal of the nitrogen accompanied by an increase of 1.6-fold of oxygen content due to thermal removing of C–N fragments. Eventually, we expect that by choosing other vapor doping agents, instead of $EtNH_2$, the heteroatoms could be further kept in the material even at higher temperatures. The doping scheme and the study via XPS would help to depict the type of bond formed via the gaseous doping agent and therefore design thin films with the desired properties and chemical composition.

3. Conclusion

m-RC thin films were synthesized in a simple test tube approach via carbon suboxide obtained from phosphorus pentoxide and malonic acid. The m-RC thin films have been exploited as a platform for amine sensing revealing the possibility to distinguish similar amines, such as primary, secondary, tertiary, and aromatic ones. The wide change in absorption, emission, and FTIR spectra makes the m-RC films a platform for sensing amines and at the same time a simple method for tuning the optical properties of this semiconductor material. As we proved that the change in the optical properties occurs in an irreversible manner via chemical reaction, the films were also exploited to prepare N-doped carbon thin films, by post exposure-carbonization at 400–500 °C directly at the substrate surface. This enables both the preparation of carbon and N-doped carbon thin films directly at the substrate

surface, for the development of thin film devices, such as resistive sensors, thin film catalysts, capacitors, and beyond. We believe that the materials and the methods used in this work will open the way for a new exciting and wide utilization of m-RC, carbon, and heteroatom-doped carbon materials as thin films, with a functional and easily tunable platform for wide range of applications.

Supporting Information

Supporting Information is available from the Wiley Online Library or from the author.

Acknowledgements

The authors acknowledge the Max Planck Society for funding. P.G. wants to thank Prof. Antonietti for support and inspiring discussions throughout the development of the project. Additionally, the authors would like to thank Baris Kumru, Majd Al-Naji, Francesco Brandi, Stefano Mazzanti, Nina Fechler, Paola Lova, Tobias Heil, Heike Runge, and Bolortuya Badamdorj for useful discussion, help with characterization, and support. Furthermore, the authors thank Dr. Axel Knop-Gericke for access to operando XPS.

Open access funding enabled and organized by Projekt DEAL.

Conflict of Interest

The authors declare no conflict of interest.

Data Availability Statement

The data that support the findings of this study are available from the corresponding author upon reasonable request.

Keywords

doping, optical properties, red carbon, thin films, vapor sensing

Received: April 15, 2022
Revised: May 16, 2022
Published online: June 27, 2022

[1] P. Giusto, H. Arazoe, D. Cruz, P. Lova, T. Heil, T. Aida, M. Antonietti, *J. Am. Chem. Soc.* **2020**, *142*, 20883.
[2] K. Sakaushi, M. Antonietti, *Acc. Chem. Res.* **2015**, *48*, 1591.
[3] N. Fechler, N. P. Zussblatt, R. Rothe, R. Schlögl, M. G. Willinger, B. F. Chmelka, M. Antonietti, *Adv. Mater.* **2016**, *28*, 1287.
[4] A. Thomas, A. Fischer, F. Goettmann, M. Antonietti, J.-O. Müller, R. Schlögl, J. M. Carlsson, *J. Mater. Chem.* **2008**, *18*, 4893.
[5] P. Giusto, D. Cruz, T. Heil, H. Arazoe, P. Lova, T. Aida, D. Comoretto, M. Patrini, M. Antonietti, *Adv. Mater.* **2020**, *32*, 1908140.
[6] A. Savateev, I. Ghosh, B. König, M. Antonietti, *Angew. Chem., Int. Ed.* **2018**, *57*, 15936.
[7] N. A. Travlou, M. Seredych, E. Rodríguez-Castellón, T. J. Bandosz, *Carbon* **2016**, *96*, 1014.
[8] L. B. Dashkevich, V. Beilin, *Russ. Chem. Rev.* **1967**, *36*, 391.
[9] T. Kappe, E. Ziegler, *Angew. Chem. Int. Ed. English* **1974**, *13*, 491.
[10] P. Giusto, *Thesis*, Universität Potsdam, **2020**.
[11] auf J. S. der Günne, J. Beck, W. Hoffbauer, P. Krieger-Beck, *Chem. Eur. J* **2005**, *11*, 4429.
[12] T. Carofiglio, L. Pandolfo, G. Paiaro, *Eur. Polym. J.* **1986**, *22*, 491.
[13] O. Diels, G. Meyerheim, *Ber. Dtsch. Chem. Ges.* **1907**, *40*, 355.
[14] E. Ziegler, in *Uber Die Konstitutionellen Beziehungen Zwischen Polypyrono-Verbindungen Und Der Roten Kohle*, Angewandte Chemie-International edition, Wiley-VCH, Weinheim, Germany **1960**, pp 582–582.
[15] J. Wang, D. Li, Y. Ye, Y. Qiu, J. Liu, L. Huang, B. Liang, B. Chen, *Adv. Mater.* **2021**, *33*, 2008020.
[16] H. Megahd, C. Oldani, S. Radice, A. Lanfranchi, M. Patrini, P. Lova, D. Comoretto, *Adv. Opt. Mater.* **2021**, *9*, 2002006.
[17] Z. Ma, P. Chen, W. Cheng, K. Yan, L. Pan, Y. Shi, G. Yu, *Nano Lett.* **2018**, *18*, 4570.
[18] P. Lova, G. Manfredi, D. Comoretto, *Adv. Opt. Mater.* **2018**, *6*, 1800730.
[19] L. Guo, T. Wang, Z. Wu, J. Wang, M. Wang, Z. Cui, S. Ji, J. Cai, C. Xu, X. Chen, *Adv. Mater.* **2020**, *32*, 2004805.
[20] Z. Li, J. R. Askim, K. S. Suslick, *Chem. Rev.* **2019**, *119*, 231.
[21] N. L. Yang, A. Snow, H. Haubenstock, F. Bramwell, *Journal of Polymer Science: Polymer Chemistry Edition* **1978**, *16*, 1909.
[22] A. Snow, H. Haubenstock, N.-L. Yang, *Macromolecules* **1978**, *11*, 77.
[23] B. Karki, M. Rajapakse, G. U. Sumanasekera, J. B. Jasinski, *ACS Appl. Energy Mater.* **2020**, *3*, 8543.
[24] K. A. Mkhoyan, A. W. Contryman, J. Silcox, D. A. Stewart, G. Eda, C. Mattevi, S. Miller, M. Chhowalla, *Nano Lett.* **2009**, *9*, 1058.
[25] C. Zhang, J. Li, E. Liu, C. He, C. Shi, X. Du, R. H. Hauge, N. Zhao, *Carbon* **2012**, *50*, 3513.
[26] J. Xu, R. Zhang, J. Wang, S. Ge, F. Wen, *Mater. Lett.* **2012**, *88*, 168.
[27] F. Kerek, R. Stimac, H.-J. Apell, F. Freudenmann, L. Moroder, *Biochimica et Biophysica Acta (BBA)-Biomembranes* **2002**, *1567*, 213.
[28] R. Stimac, F. Kerek, H. J. APELL, *Ann. N. Y. Acad. Sci.* **2003**, *986*, 327.
[29] A. Altomare, C. Cuocci, C. Giacovazzo, A. Moliterni, R. Rizzi, N. Corriero, A. Falcicchio, *J. Appl. Crystallogr.* **2013**, *46*, 1231.
[30] B. R. Sutherland, E. H. Sargent, *Nat. Photonics* **2016**, *10*, 295.
[31] S. Wei, Z. Li, W. Lu, H. Liu, J. Zhang, T. Chen, B. Z. Tang, *Angew. Chem., Int. Ed.* **2021**, *60*, 8608.
[32] M. Antonietti, M. Oschatz, *Adv. Mater.* **2018**, *30*, 1706836.
[33] National Institute of Standards and Technology, NIST Chemistry WebBook, SRD 69, **2018**.
[34] S. N. Faisal, E. Haque, N. Noorbehesht, W. Zhang, A. T. Harris, T. L. Church, A. I. Minett, *RSC Adv.* **2017**, *7*, 17950.